The effect of material stress-strain properties on fatigue failure

B. TOMKINS, G. SUMNER and J. WAREING
U.K.A.E.A., Reactor Fuel Element Laboratories, Springfields, Salwick, Preston, Lancs., England.

Summary
A theoretical treatment is made of the high strain fatigue mechanism of crack propagation in ductile metals, using a continuum method involving the distribution of plastic cohesive stresses at the crack tip. From the analysis, the well known low endurance fatigue laws of crack propagation and endurance (the Coffin-Manson law) are derived. The rate of crack growth at any instant is shown to depend on the bulk stress-strain properties of the material at that instant and the state of stress in the crack tip deformation zone. The basic material parameters which control the fatigue life of a metal are thus defined.

The theory has been shown to be valid for simple fatigue failure at room temperature in several metals and alloys. A particular experimental study has been made at room and elevated temperature on a stainless steel involving various combinations of fatigue and tensile straining. In particular the cases of tensile prestrain followed by fatigue cycling and fatigue cycling under a continuously increasing tensile strain have been studied and confirm the theoretical predictions of endurance under such conditions.

Introduction

In order to make the most efficient use of available materials in situations where it is necessary to design on a basis of fatigue failure, it is essential to know the dependence of fatigue endurance on material stress-strain properties. It is now known that fatigue is primarily a crack propagation process, a propagating crack being present from the first few percent of the life of a component. Thus, it is the crack propagation process which must be understood and analysed if the endurance of a component is to be related to the applied alternating stress-strain field and the material properties.

When a crack in a ductile metal is loaded by an applied tensile stress field, the stress intensification at the crack tip is relieved firstly by plastic deformation and secondly by a further small amount of crack extension. It is this small amount of crack extension which, under conditions of repeated loading, accumulates and produces failure by fatigue. The amount of crack growth per cycle is strictly controlled by the zone of intense plastic deformation ahead of the crack, whose size is in turn controlled by the applied stress field and material stress-strain properties.

Attempts have been made by Weertman [1], Bilby and Heald [2] and Lardner [3] to relate the repeated applied stress field and fatigue crack

growth rate for an ideal elastic-plastic material using the continuous dislocation model of Bilby, Cottrell and Swinden [4]. New crack surface is derived from plastic displacement and a dependence of crack growth rate on either the fourth power or square of the stress intensity factor predicted, in accord with some experimental data. The model is however limited in application to very low stress fatigue (applied stress $\ll$ yield stress).

Recently Tomkins [5] has applied a more flexible, but similar model, based on the equilibrium of plastic cohesive stress zones at a crack tip, to fatigue crack growth in both high and low stress regions. The model can be used to assess the effects of strain hardening (c.f. Rosenfield *et al.* [6]) and derive fatigue crack growth laws for ductile metals in terms of material parameters. In the present paper, the model is examined for various metals, including the effect of varying temperature, for simple high strain fatigue loading. It is then used to assess the effect of unidirectional/cyclic stress interactions on a 20%Cr-25%Ni stainless steel.

Model of the fatigue crack propagation process

In push-pull high strain fatigue, most crack propagation occurs by the Stage II mechanism (Forsyth [7]). Laird [8] has shown that this process is controlled by plastic shear flow near the crack tip and Biggs and Tomkins [9] have correlated new crack surface with plastic decohesion on the planes of maximum shear strain gradient at the tip. Stage I crack growth at lower strains is by a similar process, but only one of the two available planes of maximum shear at the crack tip is operative [10].

Biggs and Tomkins observed the Stage II process in a ductile metal directly and deduced the pattern of crack tip deformation and crack growth in a cycle as shown in Fig. 1(a)-(e). Intense plastic deformation is concentrated in narrow bands at $\pm 45°$ to the tensile axis and new crack surface is formed by shear decohesion along the inner edges of these bands only during the tensile loading part of the cycle. The shear flow is reversed during compression and no significant re-cohesion occurs.

The crack tip blunting which occurs by the concentration of intense plastic deformation in two narrow bands indicates that the material, even in the fully plastic state, relieves the crack tip stress singularity by the generation of plastic cohesive zones. Measurements of shear strain along a $45°$ line [9] show that the plastic shear strain increases as $1/r$ as the tip is approached (as predicted by plasticity theory) but levels off to a value approximately equivalent to the material tensile strength in the narrow flow band at the tip itself. The stress state around a plane strain equilibrium crack in a ductile metal even beyond yield, can thus be treated by the cohesive stress zone approach of Dugdale [11].

Now the Dugdale formulation for an equilibrium crack is dependent on a

linear material stress-strain relationship outside the cohesive zone, and in practice, the cyclic stress-strain curve for a metal follows a simple power law,

$$\Delta\sigma = k\Delta\epsilon_p{}^{\beta} \tag{1}$$

However, this can usually be approximated at higher strains by a linear hardening law so that the size of the cohesive shear stress zone (D) at maximum tensile strain ($\Delta\sigma/2$) is given approximately in terms of shear stresses ($\Delta\tau/2$), by,

$$\frac{D}{l} = \frac{\pi^2}{8}\left(\frac{\Delta\tau}{2\bar{S}}\right)^2\left[1 + \frac{\pi^2}{8}\left(\frac{\Delta\tau}{2\bar{S}}\right)^2\right] \tag{2}$$

where $\bar{S}$ is the mean stress in the cohesive zone ($\simeq$ shear tensile strength).

In terms of applied tensile stresses, this becomes,

$$\frac{D}{l} = \frac{\pi^2}{8}\left(\frac{\Delta\sigma}{2\bar{T}}\right)^2\left[1 + \frac{\pi^2}{8}\left(\frac{\Delta\sigma}{2\bar{T}}\right)^2\right] \tag{3}$$

Observation of the crack growth mechanism (Fig. 1) showed that new crack surface is formed by shear decohesion along the inner edge of the flow band, the block of material between the bands remaining relatively undeformed. Fig. 2 shows the model used to describe the crack tip region at maximum tensile stress ($\Delta\sigma/2$). Assuming that the material in the region ABC is plastically undeformed, the amount of decohesion δ is given by,

$$\delta = \Delta\gamma_p D \tag{4}$$

where $\Delta\gamma_p$ is the plastic shear strain applied to the bulk material during tensile loading. (Continuity of elastic strain is assumed across the cohesive zone.) However, lack of lateral constraint in the tip region for a crack propagating from an external surface leads to the crack growth per cycle being given more closely by,

$$\frac{dl}{dN} = \Delta\epsilon_p D \tag{5}$$

(It is worth noting that the crack growth per cycle is here not directly related to the plastic displacement as assumed by other investigators [1] [2] [3].)

Equations (1), (3) and (5) can be combined to give the crack growth equation in terms of either applied stress or strain range. In terms of applied strain range it is,

$$\frac{dl}{dN} = \frac{\pi^2}{8}\left(\frac{k}{2\bar{T}}\right)^2\left[1 + \frac{\pi^2}{8}\left(\frac{k}{2\bar{T}}\right)^2 \Delta\epsilon_p{}^{2\beta}\right]\Delta\epsilon_p{}^{2\beta+1} \cdot 1 \qquad (6)$$

This equation also applies to Stage I crack growth as equations (1), (3) and (5) apply equally to the Stage I process. The fatigue endurance law is given by integrating equation (6) to give,

$$\frac{\pi^2}{8}\left(\frac{k}{2\bar{T}}\right)^2\left[1 + \frac{\pi^2}{8}\left(\frac{k}{2\bar{T}}\right)^2 \Delta\epsilon_p{}^{2\beta}\right]\Delta\epsilon_p{}^{2\beta+1} \cdot N_f = \ln\left(\frac{l_f}{l_0}\right) \qquad (7)$$

As $\ln(l_f/l_0)$ is approximately constant, except at very high strains, equation (7) reduces to the well known Coffin-Manson law,

$$\Delta\epsilon_p N_f{}^{\alpha} = \text{constant} \qquad (8)$$

where $\alpha = 1/(2\beta + 1)$.

From equation (7), it can be seen that endurance is a function of only material (β, k and $\bar{T}$) and crack length (l_0 and l_f) parameters. The work of Grosskreutz [12] indicates that embryo cracks begin to propagate as cracks at a length of ~10μ. In the following work, l_0 will be taken as 10μ and l_f as a typical specimen diameter 0·25 in (6250μ).

The material parameters k and β are given by the cyclic stress strain relationship and $\bar{T}$ is approximated by the tensile strength of previously cycled material. This is often equivalent to the 'tensile strength' of the cyclic stress strain curve, i.e. $\bar{T} = \frac{1}{2}k(2\beta)^{\beta}$. Equation (7) then becomes dependent on β alone, i.e.

$$\frac{\pi^2}{8}\left(\frac{1}{2\beta}\right)^{2\beta}\left[1 + \frac{\pi^2}{8}\left(\frac{\Delta\epsilon_p}{2\beta}\right)^{2\beta}\right]\Delta\epsilon_p{}^{2\beta+1} \cdot N_f = \ln\left(\frac{l_f}{l_0}\right) \qquad (9)$$

In the following sections, the validity of the crack growth law and endurance relationships given by equations (7) and (9) will be tested by considering the effect of varying material parameters, induced by varying material, temperature or degree of hardening.

Application to various metals

For many pure metals and simple alloys, a simple endurance relationship of the form given by equation (8) has been shown to hold experimentally. In Fig. 3, theoretical curves have been drawn using equation (7) with the

tensile strength for $\bar{T}$ (this gives a lower bound for fatigue hardening materials) and equation (9), for the pure metals, copper and nickel and the simple alloys, mild steel and 310 stainless steel. The relevant material parameters for these materials are given in Table 1. The theoretical curves all lie parallel to the line of best fit through the experimental points and equation (9) is a very good fit for copper and mild steel. For nickel and 310 stainless steel it is an upper bound to the points, giving endurances a factor of 2 upon those observed. The theoretical curves show that if the correct value of $\bar{T}$ is used in equation (7), then endurances at all applied strain ranges can be accurately predicted. The theory does show how the slope and position of the endurance relationship are related to material parameters.

Some materials (e.g. aluminium, magnesium) do not have a cyclic stress - strain curve of simple power law form. In such cases, Tomkins [5] has shown that variations in the cyclic stress-strain curve are reproduced in the strain range-endurance curve in the way predicted by equation [6], i.e. a steepening of the cyclic stress-strain curve leads to a levelling off of the strain range-endurance curve and vice versa.

Effect of variation in temperature

The effect of increasing temperature for a particular material is to lower β, k and $\bar{T}$, thus increasing the slope of the Coffin-Manson line and lowering its position. Hence, for testing at a given strain range, the endurance is reduced. Sumner [13] has tested an austenitic stainless steel (20%Cr-25%Ni) in push-pull high strain fatigue at temperatures of 25 °C, 650 °C and 750 °C. The experimental results are shown in Fig. 4 along with theoretical predictions from equation (7). $\bar{T}$ is taken as the tensile strength determined from tensile tests on previously cycled material, and the values of β, k and $\bar{T}$ used are given in Table 2. The scatter in results is due to the effect of small variations in carbon content of different batches of steel used in the test programme which produce variations in the strength parameter $\bar{T}$. The lines have been drawn for one typical value of $\bar{T}$ and they can be seen at all temperatures to be a good fit to some of the experimental data.

Effect of combinations of unidirectional and fatigue straining

Combinations of unidirectional and fatigue straining present a means of varying material and crack length parameters for the same material operating at a given temperature. Also, in practical applications of materials it is sometimes important to know the effect of cycling history on tensile ductility and the effect of tensile prestrain history on fatigue endurance.

Weiss [14] and his co-workers have considered this problem experimentally and concluded that the primary effect of fatigue cycling is the initiation and propagation of a crack and the deformation processes which affect the material parameters, e.g. prestrain, are important only in so far as they affect the fracture processes. This observation is in line with the approach of the present model, whose behaviour will now be examined under such combinations of loading.

Three types of straining pattern are assessed; fatigue cycling at a given strain range followed by a tensile strain to fracture, a tensile prestrain followed by cycling at a given strain range to failure and a cycling process which involves cycling at a given strain range under a continuously increasing tensile strain—a ratchetting cycle. Supporting experimental work is on the same 20/25 austenitic steel as that used by Sumner in his earlier work and all tests are at 750°C.

Fatigue cycling followed by tensile strain

A specimen (initial diameter D_0) is cycled to a fraction (N_x/N_f) of its endurance (N_f) at the particular strain range before being strained in tension to fracture. At the end of cycling, the primary fatigue crack will have grown in length from l_0 to l_x. Hence, during the subsequent tensile strain, the effective initial diameter of the specimen is $D_x = (D_0 - l_x)$. If this diameter is pulled down to D_{x_1} at fracture compared with D_T at fracture on an uncycled specimen, the material fracture strain ϵ_T is given by,

$$\epsilon_T = 2 \ln\left(\frac{DT}{D_0}\right) = 2 \ln\left(\frac{D_{x_1}}{D_x}\right) \tag{10}$$

and the observed fracture strain (residual ductility) ϵ_R is given by,

$$\epsilon_R = 2 \ln\left(\frac{D_{x_1} + l_x}{D_0}\right) \tag{11}$$

Now for cycling at a given strain range, equation (7) can be written,

$$\ln (l_f/l_0) = KN_f \tag{12a}$$

and

$$\ln (l_x/l_0) = KN \tag{12b}$$

Assuming the values for l_f (= D_0 = 0·250 in) and l_0 (= 10μ) taken previously, equations (12a) and (12b) can be combined to give,

$$\frac{l_x}{l_f} = \exp\left[-6{\cdot}45\left(1 - \frac{N_x}{N_f}\right)\right] \tag{13}$$

Then from equations (10), (11) and (13),

$$\frac{\epsilon_R}{\epsilon_T} = \frac{\ln \{D_T + (D_0 - D_T) \exp[-6{\cdot}45\,(1 - N_x/N_f)]\} - \ln D_0}{\ln D_T - \ln D_0} \tag{14}$$

Now from simple tensile tests on 20/25 at 750 °C, for D_0 = 0·250 in, D_T = 0·116 in and hence equation (14) can be plotted as ϵ_R/ϵ_R vs N_x/N_f. This is done in Fig. 5. This theoretical curve is independent of cycling strain range and experimental results are shown for prior cycling at two strain ranges; $\Delta\epsilon_p$ = 0·048, N_f = 88 and $\Delta\epsilon_p$ = 0·0064, N_f = 800. The theoretical curve is a good fit to the experimental results and is of a form similar to the line of best fit through the experimental, results reported by Weiss. The often noted observation that prior cycling has little effect on residual ductility until most of the fatigue life has been used is seen to be due to the presence of a logarithmic crack propagation law.

Tensile prestrain followed by fatigue cycling

A specimen is prestrained to a fraction (ϵ_R/ϵ_R) of its tensile ductility before being cycled to failure at a given strain range in a fraction (N_x/N_f) of the endurance (N_f) of annealed material. The effect of the prestrain on material stress-strain parameters is to increase the average stress range $\Delta\sigma$ observed during cycling at a given $\Delta\epsilon_p$. The effect on crack length parameters is to reduce l_f from D_0 to l_x, which is the diameter after prestrain (= D_x). $\bar{T}$ and l_0 may vary slightly but can be assumed to be unchanged. Now for the material studied, it has been found that $\Delta\sigma$ varies linearly with prestrain fraction ϵ_R/ϵ_T from the value given by the cyclic stress strain curve for cycling at the particular $\Delta\epsilon_p$ (i.e. $\Delta\sigma_0$) when ϵ_R/ϵ_T = 0, to $2\bar{T}$ when ϵ_R/ϵ_T = 1. Then,

$$\Delta\sigma = (2\bar{T} - \Delta\sigma_0)\,\epsilon_R/\epsilon_T + \Delta\sigma_0 \tag{15}$$

For crack propagation after the prestrain, from equation (7),

$$\ln\left(\frac{l_f}{l_0}\right) = \frac{\pi^2}{8}\left(\frac{\Delta\sigma_0}{2\bar{T}}\right)^2\left[1 + \frac{\pi^2}{8}\left(\frac{\Delta\sigma_0}{2\bar{T}}\right)^2\right]\Delta\epsilon_p N_f \tag{16a}$$

and,

$$\ln\left(\frac{l_x}{l_0}\right) = \frac{\pi^2}{8}\left(\frac{\Delta\sigma}{2\bar{T}}\right)^2\left[1 + \frac{\pi^2}{8}\left(\frac{\Delta\sigma}{2\bar{T}}\right)^2\right] \cdot \Delta\epsilon_p N_x \tag{16b}$$

Now, $\epsilon_R = 2 \ln (l_x/l_f)$ and hence, from equations (15) and (16),

$$\frac{N_x}{N_f} = \left[1 + \frac{\epsilon_R}{2 \ln (l_f/l_0)}\right]\frac{(\Delta\sigma_0)^2[1 + \pi^2/8(\Delta\sigma_0/2\bar{T})^2]}{(\Delta\sigma)^2[1 + \pi^2/8(\Delta\sigma/2\bar{T})^2]} \tag{17}$$

$\Delta\sigma_0$ varies with cycling strain range $\Delta\epsilon_p$, so that a theoretical curve given by equation (17) is obtained for each $\Delta\epsilon_p$ considered. In Fig. 6, equation

(17) is plotted for the two strain ranges used previously ($\Delta\epsilon_p$= 0·048 and 0·0064). The experimental results are also shown in this figure and, although showing scatter, follow the predicted trend. The results are consistent with the theory, which predicts that cycling at a lower strain range after a given prestrain results in a reduction in fractional endurance. The curve is of a different form to that for tensile strain following fatigue cycling.

Fatigue cycling under a continually increasing tensile strain

In a ratchetting type of cycle, the specimen is cycled at a constant strain range whilst the mean strain in the specimen is increased at a constant rate. The specimen can fail by either fatigue or tensile failure depending on the mean strain rate. Ratchetting can be considered in a similar way to the other types of cycle, the specimen failing at a mean strain $\epsilon_R (< \epsilon_T)$ and an endurance $N_x (< N_f)$. For a constant mean strain increment per cycle, ϵ, $\epsilon_R = N_x \epsilon$. At any time prior to failure, the mean strain ϵ_{R_i} is given by $N\epsilon$.

Firstly, the case of failure primarily by fatigue is considered. The effect of the ratchet strain is to increase $\Delta\sigma$ continuously and decrease l_f. $\Delta\sigma$ is now a function of N and equation (15) becomes,

$$\Delta\sigma = (2\bar{T} - \Delta\sigma_0)\frac{N\epsilon}{\epsilon_T} + \Delta\sigma_0 \qquad (18)$$

Using equation (7) and integrating in a similar way to that used in the previous section, but with $\Delta\sigma$ as a function of N, an equation corresponding to equation (17) is derived, namely,

$$\frac{N_x}{N_f}\left\{(\Delta\sigma_x)^3\left[1+\frac{3}{5}\frac{\pi^2}{8}\left(\frac{\Delta\sigma_x}{2\bar{T}}\right)^2\right]-(\Delta\sigma_0)^3\left[1+\frac{3}{5}\cdot\frac{\pi^2}{8}\left(\frac{\Delta\sigma_0}{2\bar{T}}\right)^2\right]\right\}$$

$$=\frac{\epsilon_R}{\epsilon_T}\frac{3}{(2\bar{T}-\Delta\sigma_0)}\left[1+\frac{\epsilon_R}{2\ln(l_f/l_0)}\right]\cdot\Delta\sigma_0^2\left[1+\frac{\pi^2}{8}\left(\frac{\Delta\sigma_0}{2\bar{T}}\right)^2\right] \qquad (19)$$

where $\Delta\sigma_x$ is the stress range corresponding to a mean strain ϵ_R. Equation (18) has been plotted in Fig. 7. As expected, it is similar in form to the curves in Fig. 6 but shows a longer fractional endurance for cycling at a given strain range. Experimental points where failure is primarily by fatigue ($\Delta\epsilon_p$ = 0·048) are shown in Fig. 7 and are a good fit to the predicted curve. They fall slightly short of the curve because tensile failure does intervene on the last cycle to cause rupture (although failure is primarily by fatigue) and hence N_x is less than that calculated.

The second case, that of failure primarily by tensile fracture, which occurs when the mean strain rate is high leads to a curve almost identical to the case discussed first, that of fatigue followed by tensile strain to fracture. The theoretical curve from Fig. 5 is therefore plotted in Fig. 7 over the region where it holds. An experimental point for this type of failure is shown in Fig. 7. The effect on Fig. 7 of cycling at a different $\Delta\epsilon_p$ will be similar to that shown in Fig. 6.

Conclusions

The model developed is a simple one, but one based on experimental observations of the fatigue crack growth process. It predicts the observed effect of variation in material properties and offers an approach to assessing and comparing the expected fatigue behaviour of different materials under different conditions. It also indicates the parameters which must be changed to enhance the fatigue properties of a particular metal.

The model has been shown to be applicable to combinations of fatigue and unidirectional straining and is therefore useful in assessing the effects of prestrain and varying mean strain on fatigue. It is also useful in determining the effect of fatigue damage on the load bearing capacity and ductility of a metal component.

Acknowledgements

This paper is published by permission of Mr R. V. Moore, Managing Director of the Reactor Group of the United Kingdom Atomic Energy Authority.

References

1. WEERTMAN, J. 'Rate of growth of fatigue cracks calculated from the theory of infinitesimal dislocations distributed on a plane', *Int. J. Fract. Mech.*, vol. 2, p. 460, 1966.
2. BILBY, B. A. and HEALD, P. T. 'Crack growth in notch fatigue', *Proc. Roy. Soc. (A)*, vol. 305, p. 429, 1968.
3. LARDNER, R. W. 'A dislocation model for fatigue crack growth in metals', *Phil. Mag.*, vol. 17, No. 145, p. 71, 1968.
4. BILBY, B. A., COTTRELL, A. H. and SWINDEN, K. H. 'The spread of plastic yield from a notch', *Proc. Roy. Soc. (A)*, vol. 272, p. 304, 1963.
5. TOMKINS, B. 'Fatigue crack propagation—an analysis', *Phil. Mag.*—in press.
6. ROSENFIELD, A. R., DAI, P. K. and HAHN, G. T. 'Crack extension and propagation under plane stress', *Int. Conf. on Fracture*, Sendai, Japan, 1965.
7. FORSYTH, P. J. E. 'A two stage process of fatigue crack growth', Crack Propagation Symposium, Cranfield, p. 76, 1961.
8. LAIRD, C. 'The influence of metallurgical structure on the mechanisms of fatigue crack propagation', Fatigue crack propagation Symposium (ASTM STP 415), p. 131, 1967.

9. BIGGS, W. D. and TOMKINS, B. 'Low endurance fatigue in metals and polymers—II the mechanisms of failure', *J. Metls. Sci.*—in press.
10. KAPLAN, H. I. and LAIRD, C. 'On the mechanism of stage I crack propagation in fatigue', *Trans. Met. Soc. A.I.M.E.*, vol. 239, p. 1017, 1967.
11. DUGDALE, D. S. 'Yielding of steel sheets containing slits', *J. Mech. Phys. Solids*, vol. 8, p. 100, 1960.
12. GROSSKREUTZ, J. C. 'Fatigue crack propagation in aluminium single crystals', *J. Appl. Phys.*, vol. 33, p. 1787, 1962.
13. SUMNER, G. 'The low endurance fatigue behaviour of a 20% Cr-25% Ni-0·7% Nb stainless steel at 25, 650 and 750°C.' Int. Thermal and High Strain Fatigue Conf., London, 1967.
14. WEISS, V. 'Analysis of crack propagation in strain cycling fatigue'. Fatigue—an interdisciplinary approach, *Syracuse Univ. Press*, p. 179, 1964.

Table 1

Material	β	*k (psi)*	*Tensile strength (lb/in²)*
Cu	0·237	158,000	51,500
Ni	0·306	483,000	120,000
MS	0·236	307,000	79,000
310SS	0·288	475,000	93,000

Table 2

Temperature (°C)	β	*k (psi)*	$\bar{T}$ *(psi)*
25	0·254	370,000	116,000
650	0·216	210,000	73,100
750	0·185	130,000	46,700

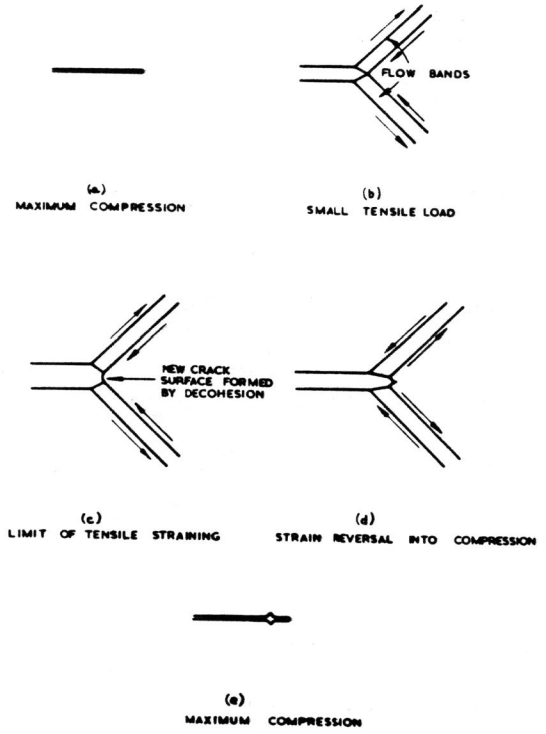

Fig. 1. The stage II crack propagation process in a metal (Ref. 5).

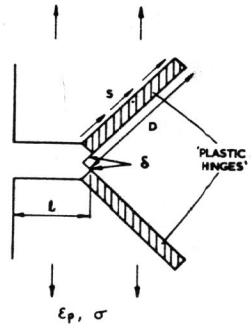

Fig. 2. Model of stage II process for analysis (Ref. 5).

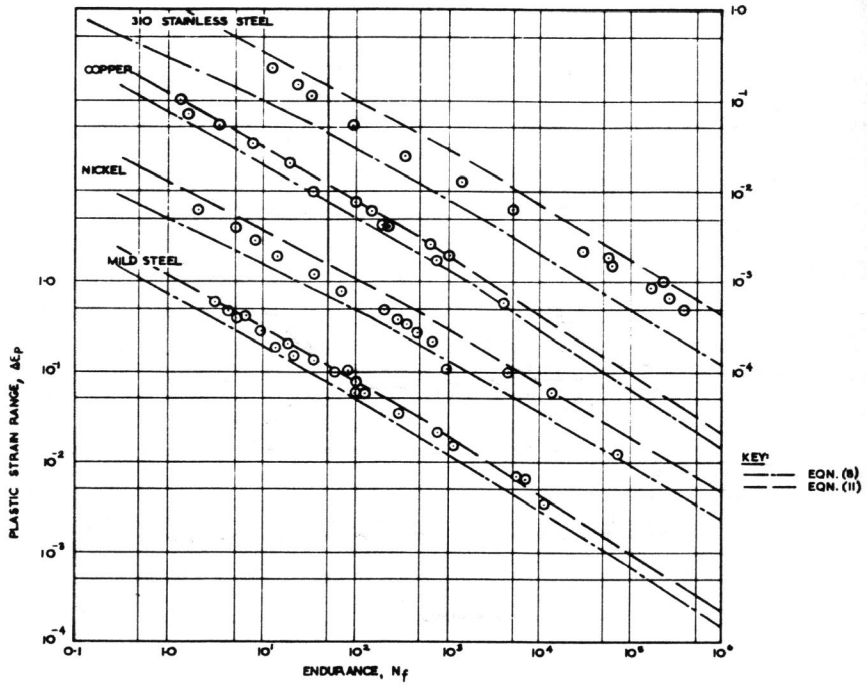

Fig. 3. Predicted fatigue behaviour of various metals.

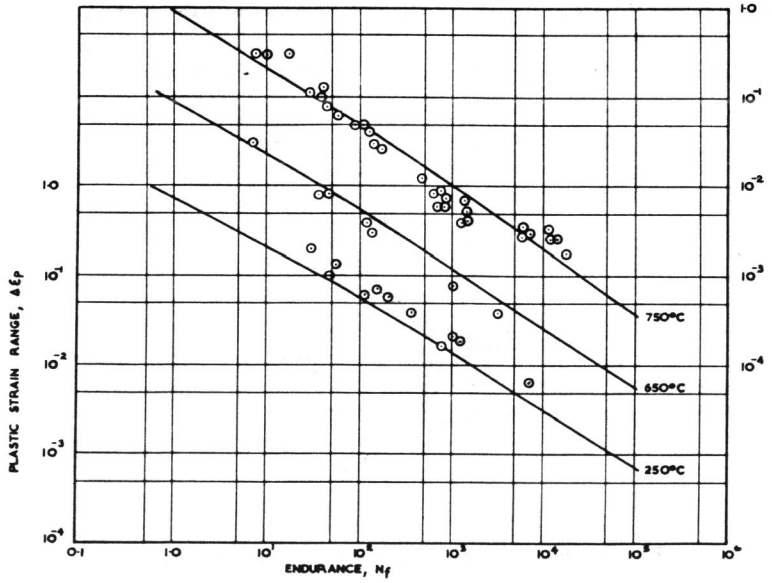

Fig. 4. Predicted fatigue behaviour of a 20% Cr-25% Ni stainless steel at room and elevated temperatures.

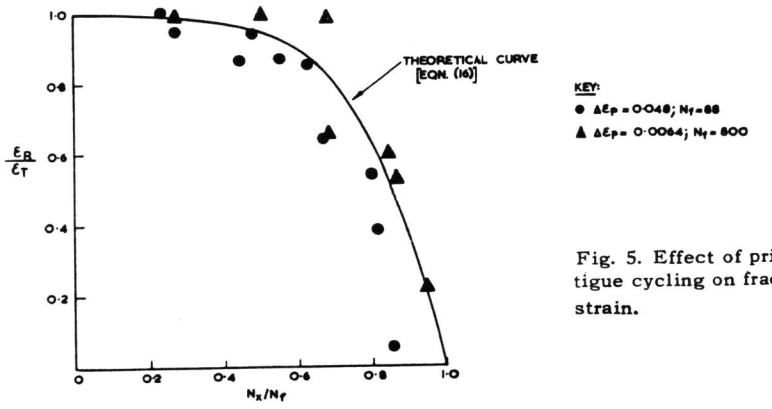

Fig. 5. Effect of prior fatigue cycling on fracture strain.

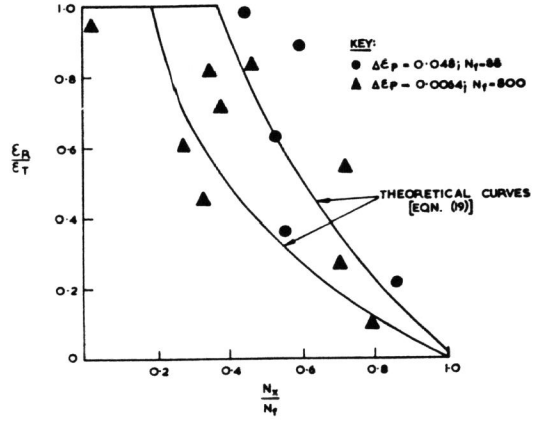

Fig. 6. Effect of tensile prestrain on fatigue endurance.

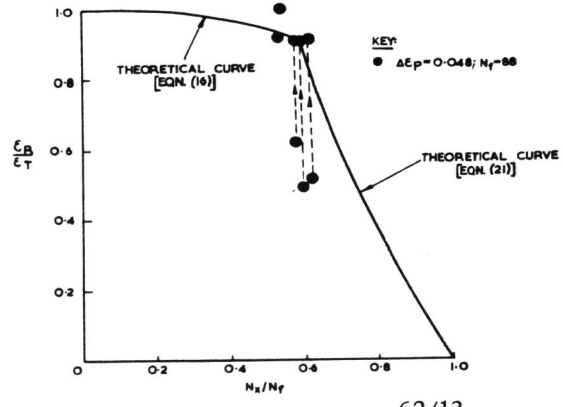

Fig. 7. Effect of combination of fatigue cycling and continuously increasing tensile strain.